COMPUTATIONAL PLACENTAL PATHOLOGY: USING PLACENTAL GEOMETRY TO ASSESS PLACENTAL FUNCTION

by

Jenny Li

B.Sc., Simon Fraser University, 2004

A PROJECT SUBMITTED IN PARTIAL FULFILLMENT
OF THE REQUIREMENTS FOR THE DEGREE OF
MASTER OF SCIENCE
IN THE
DEPARTMENT OF MATHEMATICS

SIMON FRASER UNIVERSITY
Spring 2009

APPROVAL

Name: Jenny Li

Degree: Master of Science

Title of project: Computational Placental Pathology: Using Placental Geometry to Assess Placental Function

Examining Committee: Dr. David Muraki
Chair

Dr. Adam Oberman
Senior Supervisor

Dr. Sandy Rutherford
Supervisor

Dr. JF Williams
Internal Examiner

Date Approved: _____

Abstract

Placental pathologists diagnose disease based on examining the placenta. It is hypothesized that poor blood vessel coverage may be detrimental to fetal development and may lead to low birth weight. In this project, geometrical measures of the placental structure are computed based on the total area of vessels and the vessel coverage on an important part of the placenta known as the chorionic plate. Vessel coverage is measured by the average of the distance from every point on the chorionic plate of the placenta to the closest vessel. The distance is computed using the fast sweeping method for the eikonal equation. These measures are studied for correlation with birth weight. Additionally, various image processing techniques are investigated for use on digital placental images.

Keywords:

Medical images, placental pathology, eikonal equation, distance function, scientific computing

Acknowledgments

The research behind this project was supported financially by a MITACS ACCELERATE Canada internship.

I sincerely thank Dr. Alexander Rutherford and Dr. JF Williams for believing in my ability and having faith in me. Thanks to Dr. Adam Oberman and Dr. Carolyn Salafia for introducing me to this interesting project. I also thank my family and friends for their support.

Contents

Approval ii

Abstract iii

Acknowledgments iv

Contents v

List of Tables vii

List of Figures viii

1 Introduction 1

1.1 General Background 1

1.1.1 Biological Background 1

1.1.2 Computer Assisted Pathology 2

1.2 Introduction to the Problem 3

1.2.1 Problem on the Chorionic Plate 3

1.2.2 Problem on Histology Slide 4

2 Coverage of the Chorionic Plate 6

2.1 Problem Setting 6

2.2 Distance to Blood Vessels 7

2.2.1 The Eikonal Equation 7

3 Numerical Implementation 10

3.1 Numerical Schemes 10

3.1.1 Artificial time . . . 11
3.1.2 Iterative methods . . . 11
3.1.3 Fast Sweeping method . . . 13
3.2 Boundary Conditions . . . 14
3.3 Initial Conditions . . . 17
3.4 Stopping Conditions . . . 17

4 Results **18**
4.1 Comparison of Numerical Schemes in 1D . . . 18
4.2 Comparison of Numerical Schemes in 2D . . . 23
4.3 Distance on the Chorionic Plate . . . 23
4.4 Geometric Analysis . . . 23
4.5 Data Analysis . . . 27
4.5.1 Correlation Study . . . 27
4.5.2 Correlation Example . . . 28
4.5.3 Correlation of Real Data . . . 29

5 Image Segmentation **30**
5.1 Manual Segmentation . . . 30
5.2 De-blurring . . . 31
5.3 De-noising . . . 31
5.4 Segmentation . . . 34
5.4.1 Active Contours (Snakes) Method . . . 35
5.4.2 Active Contours without Edges . . . 35
5.5 Shape-from-shading . . . 36

6 Conclusions **38**

Bibliography **40**

List of Tables

4.1 Comparison of numerical schemes in 1D 22
4.2 Comparison of numerical schemes in 2D 23
4.3 M1 values and mock BW data 28
4.4 Correlation study on real data 29

List of Figures

1.1 Cross-sectional view of a placenta 2
1.2 Top view of a placenta 4
1.3 Schematic top view of a placenta 4
1.4 Placenta histology slides 5

2.1 Sample vessels on a chorionic plate 6
2.2 Limitation of total vessel length measure 7
2.3 Distance to the nearest vessel 8
2.4 Distance function in 1D 8

3.1 Illustration of sweeping directions 15
3.2 Example of the fast sweeping method in 2D 16

4.1 Example of computing distance using artificial time in 1D 19
4.2 Example of computing distance using Jacobi iteration in 1D 20
4.3 Example of computing distance using Gauss–Seidel iteration in 1D 21
4.4 Example of computing distance using the fast sweeping method in 1D 22
4.5 Plot of distance to the nearest vessel with good coverage 24
4.6 Plot of distance to the nearest vessel with poor coverage 25
4.7 Scatter plot 29

5.1 De-blurring example 31
5.2 De-blurring of a placenta image 32
5.3 De-noising example 33
5.4 De-noising of a placenta image 34
5.5 Edge detection of a placenta image 35

5.6 Active contours without edges applied on a placenta image 36
5.7 Shape from shading of a placenta image 37

Chapter 1

Introduction

1.1 General Background

Medical research has shown that problems during the development of human fetuses may be associated with diseases in later life, including heart disease, stroke, diabetes, and hypertension [Bar97]. Researchers are trying to understand more about this connection by studying the placenta.

Recently, placental pathologists have examined more detailed geometric information on the placenta with the goal of relating this information to risk factors for later health. Specifically, branching of the blood vessels on the placenta may be an indication of increased risk factor for diseases in the fetus related to growth of blood vessels (multiple sclerosis) or neurons (schizophrenia) [RP07].

1.1.1 Biological Background

The placenta plays an important role in fetal development. It is the medium that transports oxygen and nutrients between the mother and the fetus.

A normal placenta is rounded in shape, which is the result of growing uniformly outward from the umbilical cord. However, the placenta develops differently into an irregular shape for various reasons in roughly one third of all pregnancies [YSS$^+$08]. This irregularity is often associated with lower birth weight of the placenta and this could potentially be a factor in diagnosing health risks for the future [YSS$^+$08].

Macroscopically, when viewed from the side as in Figure 1.1, the placenta consists of

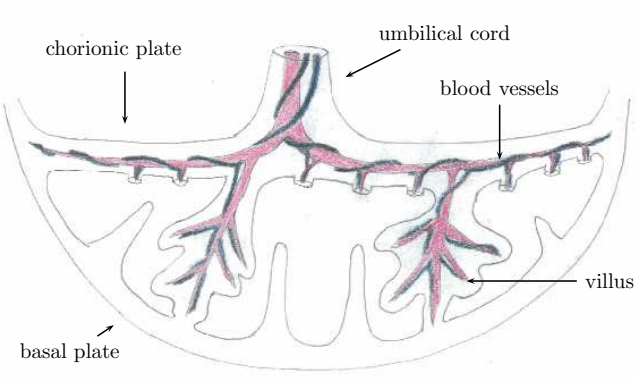

Figure 1.1: Cross-sectional view of a placenta.

two surfaces: the top surface which has the umbilical cord attached is called the chorionic plate, and the bottom surface, known as the basal plate [GNS+08].

The space between the chorionic and basal plates is filled with the maternal blood. The blood from the fetus circulates through the umbilical cord and travels through progressively finer tree structure of blood vessels in the placenta. When the fetal blood reaches the villi, nutrients are exchanged with the maternal blood.

1.1.2 Computer Assisted Pathology

Pathology is the macro- and microscopic study of cells and tissues in order to determine the cause and etiology of a disease or outcome. Placental pathology is the study of the pathology of placenta and in particular how it relates to the fetus.

The process of interpreting the size, shape and consistency of the placenta and its functional parts is often restricted to well trained pathologists [SV90]. This process is time consuming and may be rather subjective in the sense discussed in Section 5.1. We explore the use of digital image processing techniques to assist pathologists in interpreting, denoising, and analyzing geometric properties of the placenta.

Computer assisted diagnosis is the "application of computer programs designed to assist the physician in solving a diagnostic problem" [HNF08]. For example, [ACI98] presented how computers can help physicians to diagnose of pediatric rheumatic diseases.

We would like to help pathologists make diagnoses by providing computer output as

a tool to provide insight. We call this "computer assisted pathology". Ideally, computer assisted pathology would use digital images of placentas to improve detection and interpretation of blood vessel coverage, segmentation of vessels, and eventually even automatic suggestion of diagnoses for consideration by a trained pathologist. In this document, one particular aspect of computer assisted pathology is considered: the determination of placental blood vessel coverage.

1.2 Introduction to the Problem

The birth weight and age of the placenta is related to the birth weight of the fetus [SMT+05]. Beyond these factors, we investigate how information about the shape of the placenta relates to the birth weight or other fetal properties. The geometry of the placenta, size and vasculature (blood vessel) coverage may be useful indicators.

The main blood vessel branches are connected to the umbilical cord, see Figure 1.1. As the fetus and the placenta develop, these blood vessels grow and branch off into smaller vessels. The environment in which this happens can influence growth so that some blood vessels do not form or form incorrectly. In this case, the blood vessels may fail to provide adequate coverage of the placenta.

The distribution of blood vessels influences the work that must be done by the heart of the fetus in pumping blood through the placenta. The net nutrition to the fetus is equal to the amount transferred across the placenta minus the amount of energy expended by the fetus to pump the blood to and from the placenta. In order to help understand the fetal environment we study the structure of the blood vessels.

The placenta is a three dimensional object, and one could study the geometric properties such as the vasculature in 3D. For practical considerations and because the important superficial vessels appear earlier in the development, we consider two 2D problems. The first is looking at the chorionic plate only, and the second is to study cross sectional histology slides of the placenta. These two problems correspond to the available digital images.

1.2.1 Problem on the Chorionic Plate

While Figure 1.1 showed a side view, if we look down at a placenta from above, we see the chorionic plate, for example see Figure 1.2 where the blood vessels appear as a faint tree structure of connected curves of various thickness. Figure 1.3 is a schematic version of

Figure 1.2 where the blood vessels have been manually traced by a trained pathologist. The question addressed in this project is the blood vessel coverage on the chorionic plate. This problem will be developed further in the remainder of this document.

Figure 1.2: Top view of a placenta. The umbilical cord has been detached and placed next to the placenta. A penny and a ruler appear for scale.

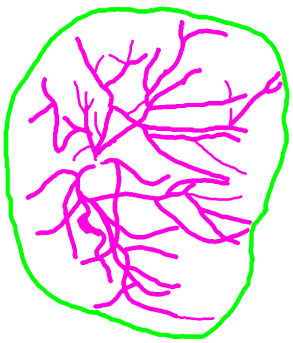

Figure 1.3: Schematic top view of a placenta with blood vessels manually traced.

1.2.2 Problem on Histology Slide

A histology slide is the result of slicing the placenta in Figure 1.1 from top to bottom, and then photographing the cross sectional image under a light microscope. The fetal blood

vessels and the connective tissue surrounding them are captured as blobs. The tissue is dyed so that different types of structures have different colors. The connective tissue forms light pink blobs while fetal blood vessels appear as smaller red blobs within pink ones. Cell nuclei appear as small blue dots (see Figure 1.4). Pathologists are interested in the relative sizes, quantities, and irregularities of the blobs and amount of white space in these images.

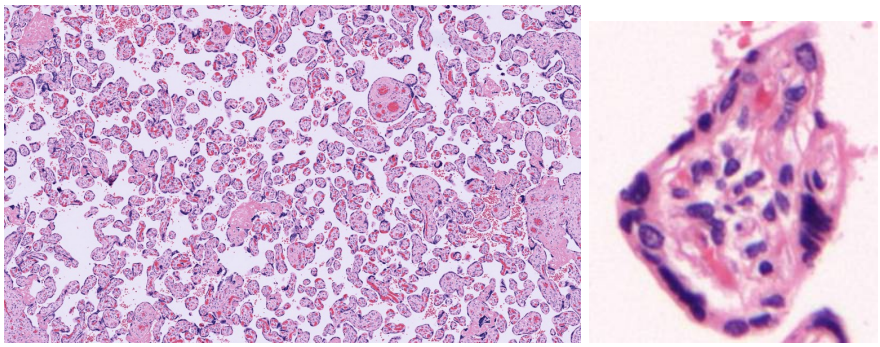

(a) 2-D Cross section placenta slide (b) Individual villous

Figure 1.4: Placenta histology slides.

This project focuses on explaining and solving the problem of computing the blood vessel coverage of the chorionic plate. The problem about the analysis of histology slides is discussed in the MITACS Summer School in Industrial Mathematics report [ABD$^+$08].

Chapter 2

Coverage of the Chorionic Plate

2.1 Problem Setting

Figure 2.1 is an schematic illustration of a chorionic plate of the placenta. We would like to have a measure for the vessel branching and coverage properties on it. This measure should tell us how well or poor the vessels coverage is, which can then perhaps be related to the overall access to nutrition for the fetus.

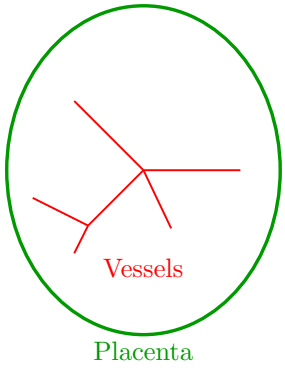

Figure 2.1: Sample vessels on a chorionic plate.

Two basic measurements of blood vessels are used:

1. Total vessel length.
2. Average distance from any point on the chorionic plate to the nearest blood vessel.

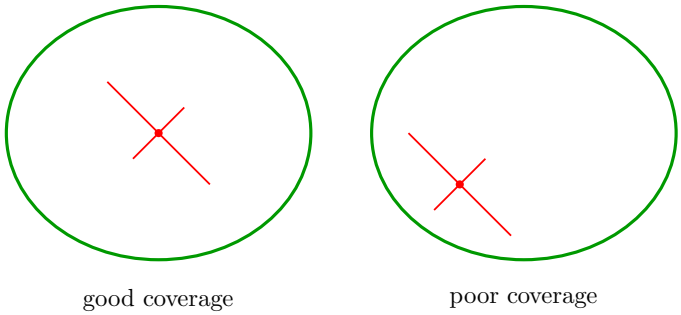

Figure 2.2: Limitation of total vessel length measure. These two images have the same total vessel length but the left one has better coverage.

The first approach is plausible, however from Figure 2.2 we can see a potential difficulty: only measuring the total length of the blood vessel does not capture differences in position for the same vessel length. Thus this project focuses mostly on the second approach. However the total length of the vessels will be used in scaling our later measurements as described in Section 4.4.

2.2 Distance to Blood Vessels

The idea is to calculate the distance $u(\vec{x})$ from any point $\vec{x}$ inside the placenta to the nearest vessel, take an average inside the placenta, then normalize to image scale. For example, we can use the average distance divided by the largest distance from the edge of the placenta. This will give us a number between 0 and 1. A smaller number indicates better blood vessel coverage.

2.2.1 The Eikonal Equation

In order to compute the distance, one approach is to study the eikonal equation with appropriate boundary conditions. The eikonal equation is a first-order Hamilton-Jacobi equation [Eva98] which can be solved numerically by various techniques. Several of these techniques will be discussed in Chapter 3.

The eikonal equation with speed 1 is

$$|\nabla u| = 1, \tag{2.1}$$

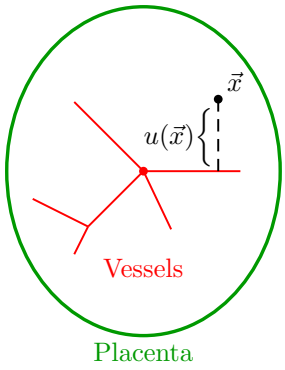

Figure 2.3: Distance to the nearest vessel.

where $u : \Omega \in \mathbb{R}^2 \to \mathbb{R}$, and $|\nabla u|$ is the length of the gradient, $\sqrt{u_x^2 + u_y^2}$.

Intuitively u represents distance because the solution to (2.1) has unit change in u for unit change in any spatial direction. The boundary conditions for the eikonal equation can used to specify values for u on a set of points Γ. The set Γ need not be the boundary of the domain Ω and in our case it will be in the interior of the domain.

In one dimension, the distance to a fixed point x_0 is $|x - x_0|$, and it is clear from Figure 2.4 that because the slope of the function is ± 1, this function is indeed a solution of the eikonal equation. Note from the figure that the solution of the eikonal equation is not smooth and in general may have discontinuous first derivatives. Here the boundary condition is $u(x_0) = 0$.

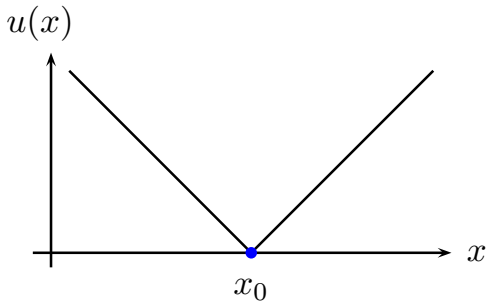

Figure 2.4: Distance function in 1D.

In two dimensions, where

$$\nabla u = \begin{bmatrix} u_x \\ u_y \end{bmatrix},$$

the eikonal equation is

$$\sqrt{u_x^2 + u_y^2} = 1. \tag{2.2}$$

This will be the form we make use of in this document.

Chapter 3

Numerical Implementation

Our goal is to numerically solve the eikonal equation $|\nabla u| = 1$, with $u = 0$ on the blood vessels where the solution u represents distance.

Some techniques include the algebraic Newton method [HT05], fast marching method [Set99], upwinding finite difference schemes with artificial time, iterative schemes such as Jacobi and Gauss-Seidel, and the fast sweeping method [TCOZ03]. This chapter explains in detail the artificial time, Jacobi, Gauss-Seidel, and the fast sweeping methods.

[GK06] compared the fast sweeping and fast marching methods, and concluded that the fast marching method is faster for problems with complicated obstacle geometry. However, the fast sweeping method is considerably simpler to implement. The boundary of the chorionic plate can be thought as an obstacle, and in most of the images, it is reasonably close to convex. The complexity of the image is in the vessel structure, and this poses no difficulty for fast sweeping method. Therefore, in this study, it is expected that fast sweeping will perform reasonably well and fast marching is not implemented.

3.1 Numerical Schemes

Because we are working with a digital image consisting of a grid of pixels, it makes sense to use a cartesian grid. We discretize the spatial domain with grid spacing Δx in the x-direction and Δy in y-direction, and for the time-dependent problem in Section 3.1.1, we discretize the temporal domain with grid spacing Δt.

Let $x_{i,j}$ denote the grid points of the computational domain, and $U_{i,j}$ denote the numerical solution at $x_{i,j}$. The digital image is $I \times J$ pixels so $i = 1 \ldots I$ and $j = 1 \ldots J$.

3.1.1 Artificial time

We explain this method first because it is easier to implement, later we explain some faster methods. Begin by introducing a time dependence,

$$u_t = 1 - \sqrt{u_x^2 + u_y^2},$$

which at steady state will agree with (2.2). This can be solved numerically in time by using the Forward Euler method. Note that because information in the solution travels along characteristic curves [Eva98], it is advantageous to use upwinding for the spatial derivatives. To obtain this, we use the max function and first-order differences to approximate u_x and u_y:

$$|U_x| = \max\left(-\frac{U_{i+1,j} - U_{i,j}}{\Delta x}, -\frac{U_{i-1,j} - U_{i,j}}{\Delta x}, 0\right),$$

$$|U_y| = \max\left(-\frac{U_{i,j+1} - U_{i,j}}{\Delta y}, -\frac{U_{i,j-1} - U_{i,j}}{\Delta y}, 0\right),$$

where $|U_x|$ and $|U_y|$ are discrete approximations to the derivatives of u at $x_{i,j}$. Then the Forward Euler method gives

$$U_{i,j}^{n+1} = U_{i,j}^n + \Delta t\left(1 - \sqrt{|U_x|^2 + |U_y|^2}\right).$$

We used $\Delta t = \frac{1}{2}\Delta x$. Initially, we set $U_{i,j}^0$ to the initial conditions as discussed in Section 3.3. After each time-step, we set $U_{i,j} = 0$ on the vessels Γ and $U_{i,j} = 200$ on the placenta boundary. Results are shown in Chapter 4.

3.1.2 Iterative methods

Here, we implement several iterative methods by using the Jacobi and the Gauss-Seidel iterations [BF00]. These approaches solve the eikonal equation (2.2) directly without introducing artificial time.

We begin by describing a discretization of equation (2.2) by following the approach of [Zha05]. For each $i \in \{2, \ldots, I-1\}$ and $j \in \{2, \ldots, J-1\}$, we solve the coupled system of nonlinear equations

$$\left[(U_{i,j} - \min(U_{i-1,j}, U_{i+1,j}))^+\right]^2 + \left[(U_{i,j} - \min(U_{i,j-1}, U_{i,j+1}))^+\right]^2 = (\Delta x)^2 = 1, \qquad (3.1)$$

where

$$(x)^+ = \begin{cases} x, & x > 0 \\ 0, & x \leq 0. \end{cases}$$

At the boundaries of the computational domain, use

$$\begin{aligned}
\left[(U_{1,j} - U_{2,j})^+\right]^2 + \left[(U_{1,j} - \min(U_{1,j-1}, U_{1,j+1}))^+\right]^2 &= 1, \text{ at left boundary } i = 1, \\
\left[(U_{I,j} - U_{I-1,j})^+\right]^2 + \left[(U_{I,j} - \min(U_{I,j-1}, U_{I,j+1}))^+\right]^2 &= 1, \text{ at right boundary } i = I, \\
\left[(U_{i,1} - \min(U_{i-1,1}, U_{i+1,1}))^+\right]^2 + \left[(U_{i,1} - U_{i,2})^+\right]^2 &= 1, \text{ at bottom boundary } j = 1, \\
\left[(U_{i,J} - \min(U_{i-1,J}, U_{i+1,J}))^+\right]^2 + \left[(U_{i,J} - U_{i,J-1})^+\right]^2 &= 1, \text{ at top boundary } j = J.
\end{aligned}$$

Jacobi iteration

To solve these coupled nonlinear equations, we consider the iterative Jacobi scheme. Initially, $U_{i,j} = 0$ on the boundary Γ consisting of the blood vessels, and $U_{i,j} \geq 0$ elsewhere. The basic idea of Jacobi iteration is that given a current approximation to the solution $U_{i,j}^{\text{old}}$ for all i, j, we solve for a improved approximation $U_{i,j}^{\text{new}}$. Then we set $U_{i,j}^{\text{old}} = U_{i,j}^{\text{new}}$ for all i, j and repeat until $|U_{i,j}^{\text{old}} - U_{i,j}^{\text{new}}|$ is smaller than a specified tolerance.

For each iteration, we know $U_{i,j}^{\text{old}}$ for all i, j over all points $x_{i,j}$, and we solve

$$\left[\left(U_{i,j}^{\text{new}} - \min(U_{i-1,j}^{\text{old}}, U_{i+1,j}^{\text{old}})\right)^+\right]^2 + \left[\left(U_{i,j}^{\text{new}} - \min(U_{i,j-1}^{\text{old}}, U_{i,j+1}^{\text{old}})\right)^+\right]^2 = 1, \qquad (3.2)$$
$$\text{for } i \in \{2, \ldots, I-1\}, \quad j \in \{2, \ldots, J-1\},$$

for $U_{i,j}^{\text{new}}$ in terms of the known $U_{i,j}^{\text{old}}$ values. The problem of solving (3.2) for $U_{i,j}^{\text{new}}$ is much easier than the original (3.1) because $U_{i,j}^{\text{new}}$ for each i, j is decoupled from all the other i, j equations.

For each i, j, we solve equation (3.2) by following the approach of [Zha05]. We note that the equation

$$[(x-a)^+]^2 + [(x-b)^+]^2 = 1,$$

can be written as

$$[\max((x-a), 0)]^2 + [\max((x-b), 0)]^2 = 1. \qquad (3.3)$$

By considering 4 cases separately: (1) $x - a > 0$ and $x - b > 0$, (2) $x - a > 0$ and $x - b < 0$,

(3) $x-a<0$ and $x-b>0$, (4) $x-a<0$ and $x-b<0$, we find equation (3.3) has solution

$$x=\begin{cases}\min(a,b)+1, & |a-b|\geq 1,\\ \frac{a+b+\sqrt{2-(a-b)^2}}{2}, & |a-b|<1.\end{cases}$$

It does not matter what order we sweep through the points $x_{i,j}$ because each $U^{\text{new}}_{i,j}$ is determined independently from the $U^{\text{old}}_{i,j}$. To start the iteration, we use the initial guess from Section 3.3.

Gauss–Seidel iteration

The initial set up for Gauss–Seidel iteration is the same as Jacobi iteration, the mostly significant difference is that there is only one copy of the matrix U, and we always use the most up-do-date neighbouring values to compute $U^{\text{new}}_{i,j}$.

One way to view Gauss–Seidel is that when solving for $U^{\text{new}}_{i,j}$ in the i,j^{th} equation, we may use a new value for some of the neighboring equations, say $U^{\text{new}}_{i-1,j}$ and $U^{\text{new}}_{i,j-1}$, because we may have already computed them. Instead of using the old values, we use these new values, solving

$$\left[\left(U^{\text{new}}_{i,j}-\min(U^{\text{new}}_{i-1,j},U^{\text{old}}_{i+1,j})\right)^{+}\right]^2+\left[\left(U^{\text{new}}_{i,j}-\min(U^{\text{new}}_{i,j-1},U^{\text{old}}_{i,j+1})\right)^{+}\right]^2=1, \qquad (3.4)$$
$$\text{for } i\in\{2,\ldots,I-1\},\quad j\in\{2,\ldots,J-1\}.$$

In order to reuse the solution technique for (3.2), it is important to have the values for $U^{\text{new}}_{i-1,j}$ and $U^{\text{new}}_{i,j-1}$ before trying to solve for $U^{\text{new}}_{i,j}$, thus the order in which we sweep through the points $x_{i,j}$ can effect the solution. Here we have chosen to sweep the whole domain from $i=1:I, j=1:J$: this guarantees that we will have the values for $U^{\text{new}}_{i-1,j}$ and $U^{\text{new}}_{i,j-1}$.

3.1.3 Fast Sweeping method

The main improvement of the fast sweeping method [TCOZ03] is to not only use Gauss-Seidel iterations, but also alternate the sweeping orders. First, we sweep through the domain using one iteration of Gauss-Seidel as described above. For the next iteration, we use a different sweeping pattern.

Information in the solution of the eikonal equation travels along characteristics [Eva98]. At least one of the sweeping directions will be ideal for the characteristics in a particular

region of the domain. When the sweeping direction is aligned with the characteristics, that sweep can update large areas of the domain with an accurate solution. This explains the small number of iterations observed for the fast sweeping method in Figure 3.2 and Section 4.1.

In 1D, there are 2 sweeping patterns: counting upwards from $i = 1$ to I and then downwards from $i = I$ down to 1. These can be denoted in "Matlab style notation" as $i = 1 : I$ and $i = I : -1 : 1$. In 2D, there are 4 sweeping patterns shown below and in Figure 3.1. After finishing the fourth pattern, we begin again with the first. The 4 sweeping patterns are

1. $i = 1 : +1 : I, j = 1 : +1 : J$,
2. $i = I : -1 : 1, j = 1 : +1 : J$,
3. $i = I : -1 : 1, j = J : -1 : 1$,
4. $i = 1 : +1 : I, j = J : -1 : 1$.

Figure 3.2 shows contour plots of an example by using the fast sweeping method to compute the distance from every point inside the ellipse to the cross-shaped object.

3.2 Boundary Conditions

There are two boundary conditions we are dealing with, one is the blood vessels, another is the boundary of the computational domain, which is a rectangle in our case.

Another complication is that we only care about the distance from every point on the chorionic plate to the nearest vessel, even though in theory we can find the distance for every point on the image, we can (and should) neglect the distance information from outside the chorionic plate. In order to deal with this, in our algorithm, we set the distance on the edge of the chorionic plate to be high enough (we used 200 in the code) and because information travel outwards from the lower value, at the end, we simply ignore the distance value higher than the edge value, i.e. 200.

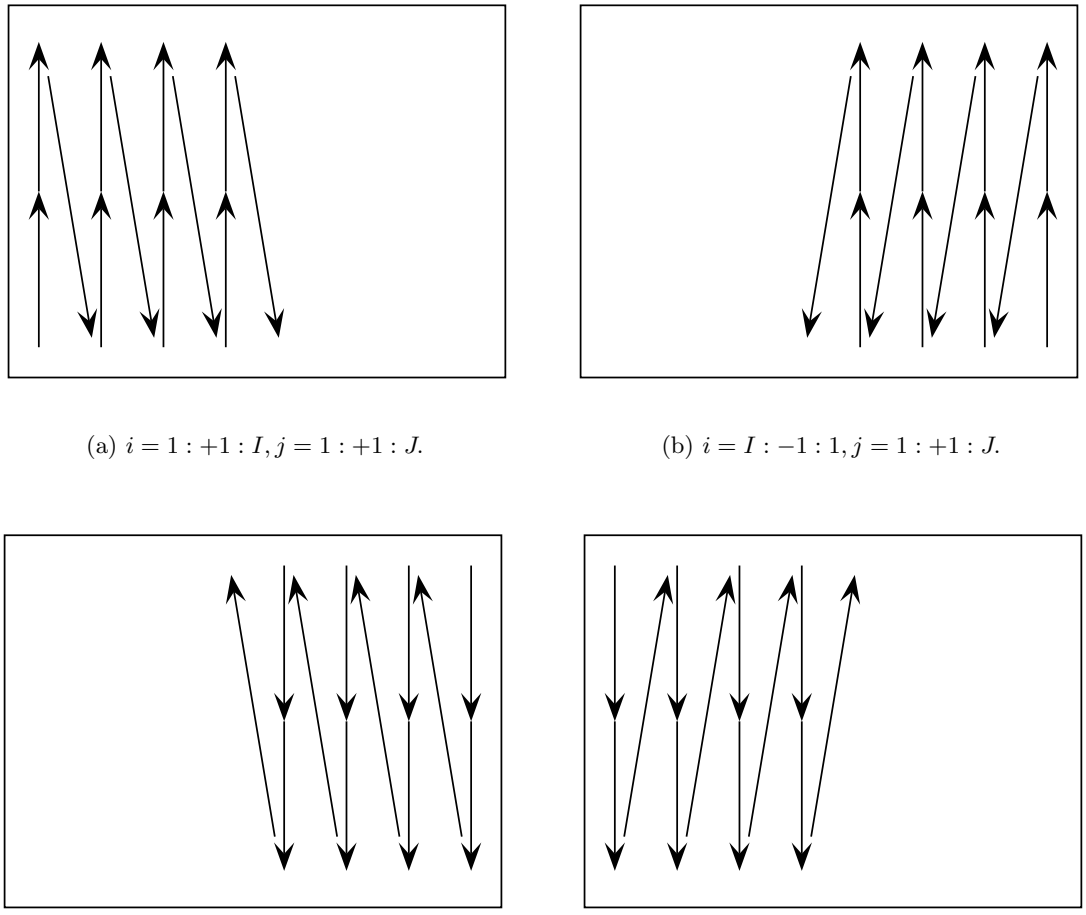

(a) $i = 1 : +1 : I, j = 1 : +1 : J$.

(b) $i = I : -1 : 1, j = 1 : +1 : J$.

(c) $i = I : -1 : 1, j = J : -1 : 1$.

(d) $i = 1 : +1 : I, j = J : -1 : 1$.

Figure 3.1: Illustration of sweeping directions.

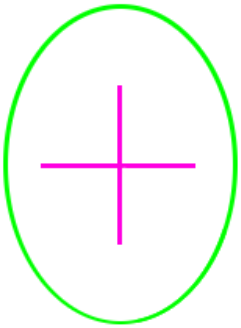

(a) Domain.

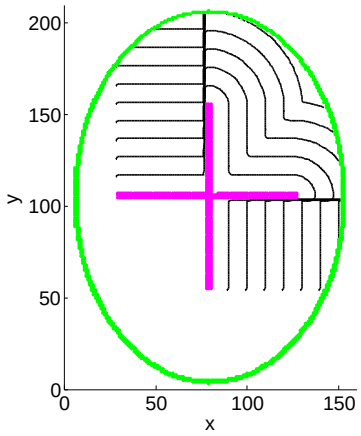

(b) 1st iteration.

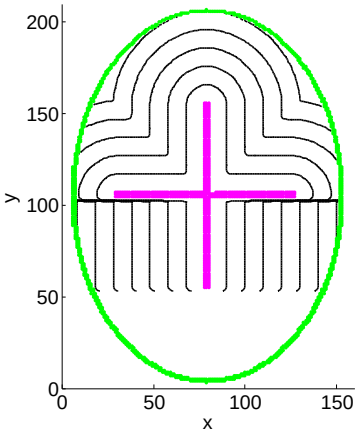

(c) 2nd iteration.

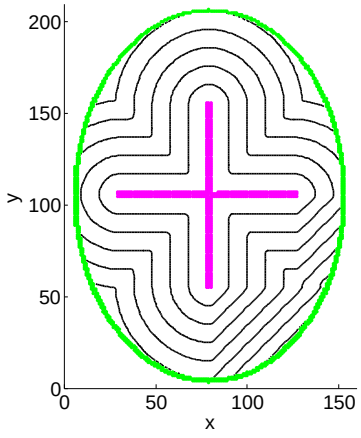

(d) 3rd iteration.

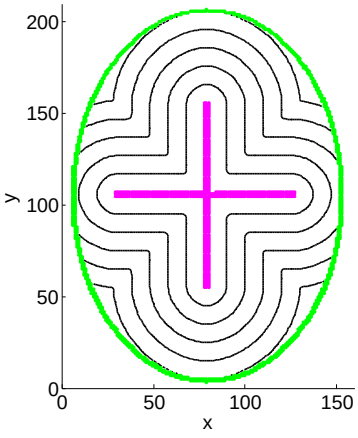

(e) 4th iteration.

Figure 3.2: 2D example of the fast sweeping method applied to an image (a). Boundary conditions of $u = 0$ are applied to the "+" sign in the interior of the ellipse. Each sweep roughly updates one quadrant. Distance is displayed using contours.

3.3 Initial Conditions

As initial conditions for the artificial time or initial guesses for the iterative schemes, we set $U_{i,j} = 0$ on blood vessels, $U_{i,j} = 200$ on the boundary of the chorionic plate and $U_{i,j} = 400$ elsewhere.

3.4 Stopping Conditions

The stopping condition here is that when the L_∞ error between the solution and the previous solution is less than a certain tolerance or threshold; in our computations, we use 10^{-10}.

Chapter 4

Results

In this chapter, we compare the numerical schemes for computing distance described in Chapter 3 on a 1D example problem and our placental images. We compute various geometric estimates of vascular coverage based on our distance computation. Some preliminary correlation with birth weight is performed.

4.1 Comparison of Numerical Schemes in 1D

We begin by computing the distance to a single point in one dimension. We compare the different schemes based on how fast they solve this problem.

Figure 4.1, 4.2, 4.3, and 4.4 illustrate a 1D example of using the artificial time, Jacobi iteration, Gauss-Seidel iteration, and fast sweeping method respectively to compute the distance to a point $x_0 = 50$ on a domain $x \in [0, 100]$.

In Figure 4.3, we note that the distance to the right of $x_0 = 50$ is computed in essentially just one iteration: this motivates the fast marching method and indeed we see in Figure 4.4 that the fast sweeping method needs only 2 iterations.

Table 4.1 shows that the fast sweeping method takes less iterations and less time to compute distance than Jacobi and Gauss-Seidel iterations. Here distance is computed to a point $x_0 = 5000$ in a domain of $x \in [0, 10000]$.

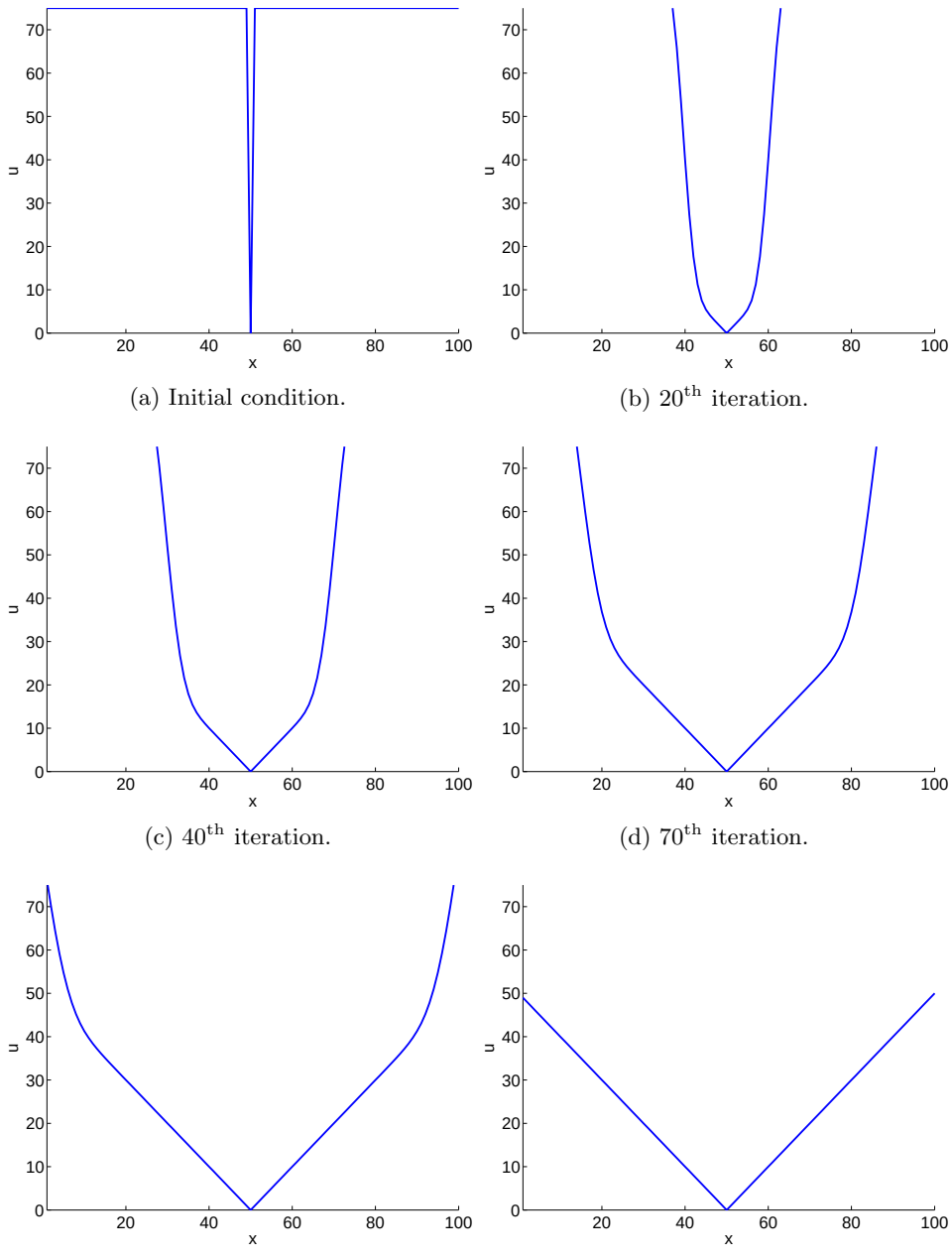

(a) Initial condition.

(b) 20^{th} iteration.

(c) 40^{th} iteration.

(d) 70^{th} iteration.

(e) 100^{th} iteration.

(f) 191^{th} iteration.

Figure 4.1: Example of computing distance using artificial time in 1D.

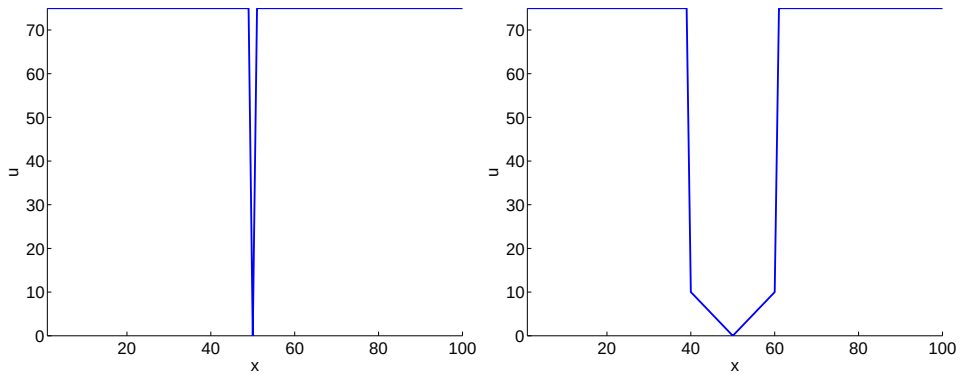

(a) Initial condition.

(b) 10^{th} iteration.

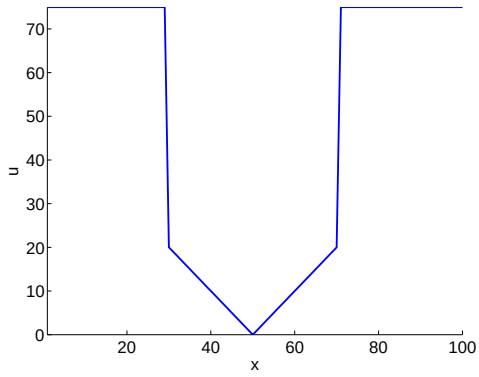

(c) 20^{th} iteration.

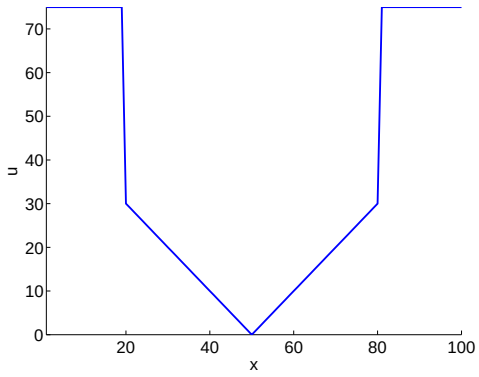

(d) 30^{th} iteration.

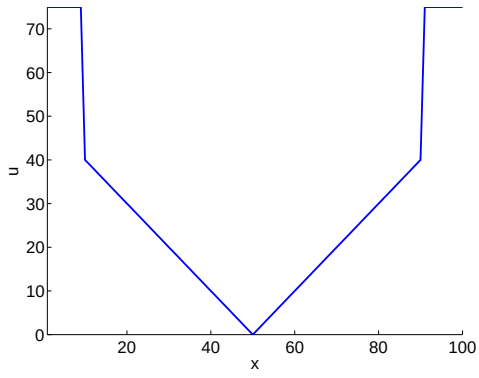

(e) 40^{th} iteration.

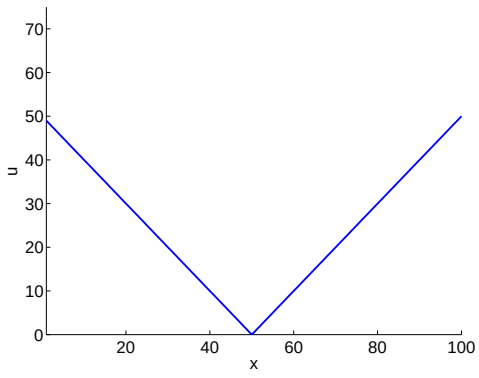

(f) 50^{th} iteration.

Figure 4.2: Example of computing distance using Jacobi iteration in 1D.

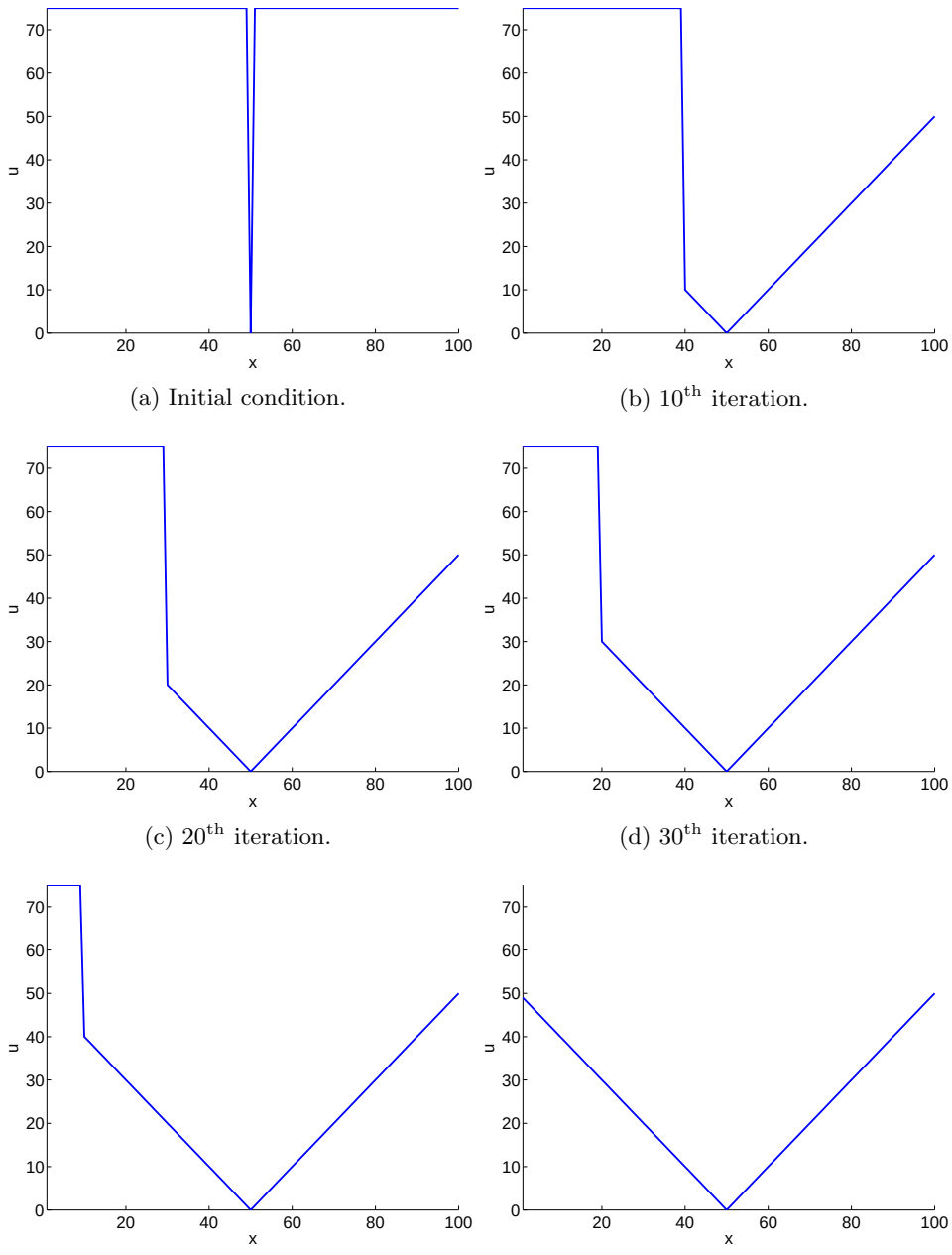

(a) Initial condition.

(b) 10^{th} iteration.

(c) 20^{th} iteration.

(d) 30^{th} iteration.

(e) 40^{th} iteration.

(f) 49^{th} iteration.

Figure 4.3: Example of computing distance using Gauss–Seidel iteration in 1D.

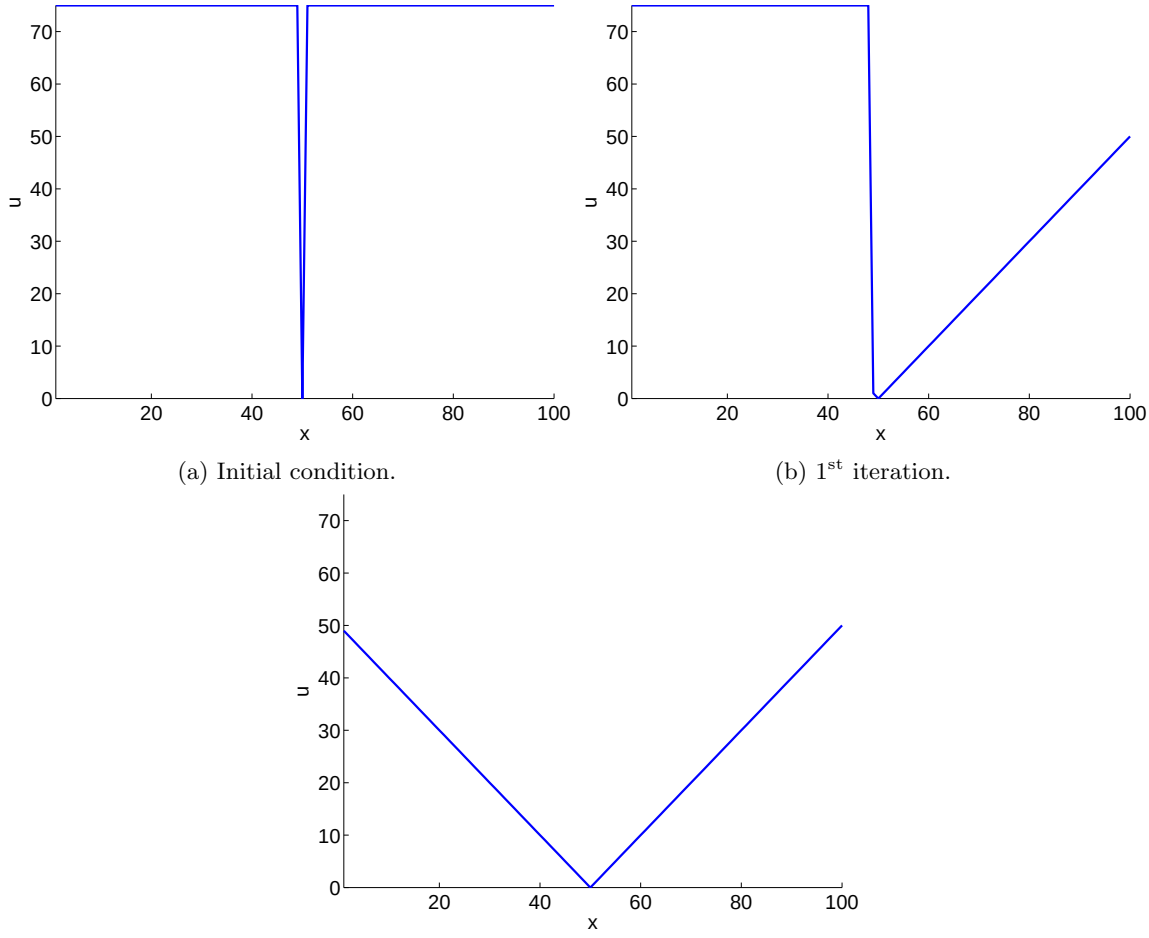

(a) Initial condition.

(b) 1st iteration.

(c) 2nd iteration.

Figure 4.4: Example of computing distance using the fast sweeping method in 1D.

	Num. of iteration	Time (s)
Artificial time	10752	24
Jacobi	5001	3
Gauss-Seidel	5000	3
Fast-sweeping	4	0.02

Table 4.1: Comparison of numerical schemes in 1D.

4.2 Comparison of Numerical Schemes in 2D

From Table 4.2, we see that the fast sweeping method performs the best for the problem of finding distance on the chorionic plate.

	Num. of iteration	Time (s)
Artificial time	885	67
Jacobi	158	7
Gauss-Seidel	154	7
Fast-sweeping	8	0.5

Table 4.2: Comparison of numerical schemes in 2D.

4.3 Distance on the Chorionic Plate

Figure 4.5 and 4.6 show the plot of distance for two particular placenta images.

As discussed in Chapter 5, it is difficult to automatically identify the blood vessels. We currently rely on marking or *segmentation* done manually by a pathologist, as explained in Section 5.1. Thus, our main focus in this Chapter is on the calculation done for the vessel coverage.

4.4 Geometric Analysis

We use the fast sweeping method to numerically solve the eikonal equation

$$|\nabla u| = 1,$$

with boundary condition $u = 0$ on the blood vessels Γ. As described in Chapters 2 and 3, this computation gives u, the distance from every point on the placenta to the closest vessel. We then take the mean of all distance values to obtain the mean distance. From this, we compute measures for vasculature coverage.

We then explore different normalizations such as scaling by the largest diameter of the placenta, by the circumference of the placenta, or by the square root of the placental area. These give us a non-dimensional number generally between 0 and 1. These values

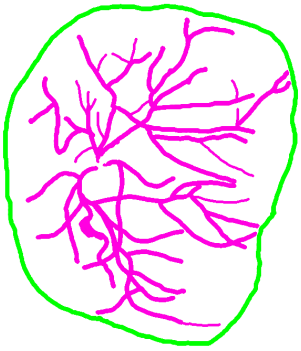

(a) Sample image with traced vessels.

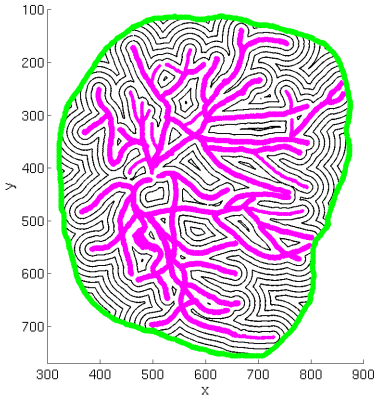

(b) Contour plot of distance.

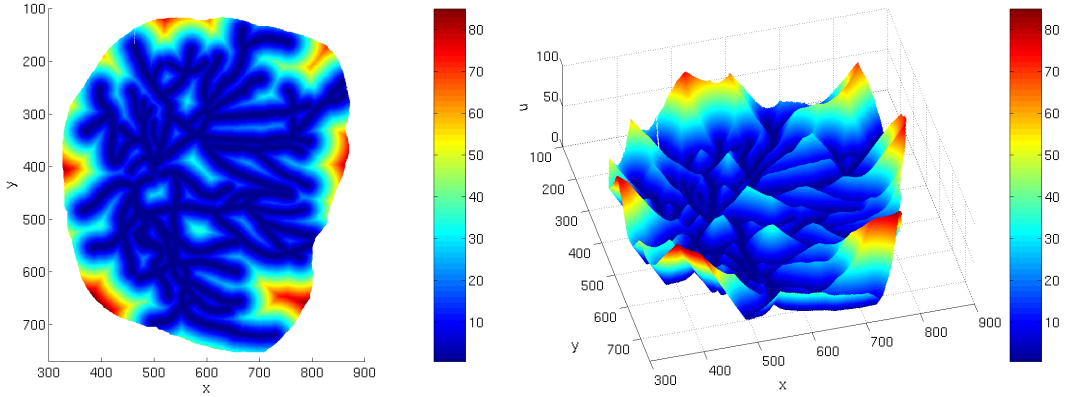

(c) Color plot of distance in 2D.

(d) Color plot of distance in 3D.

Figure 4.5: Plot of distance to the nearest vessel with good coverage.

may indicate the quality of the blood vessel coverage, where smaller numbers mean better coverage. See Section 4.5 where the measures are correlated with birth weight.

The various specific measures we consider are described next.

Mean distance Mean distance is calculated by solving the eikonal equation by one of the methods described above and then averaging over all points inside the chorionic plate. We denote this as

$$\bar{u} = \text{mean}_x(u(x)).$$

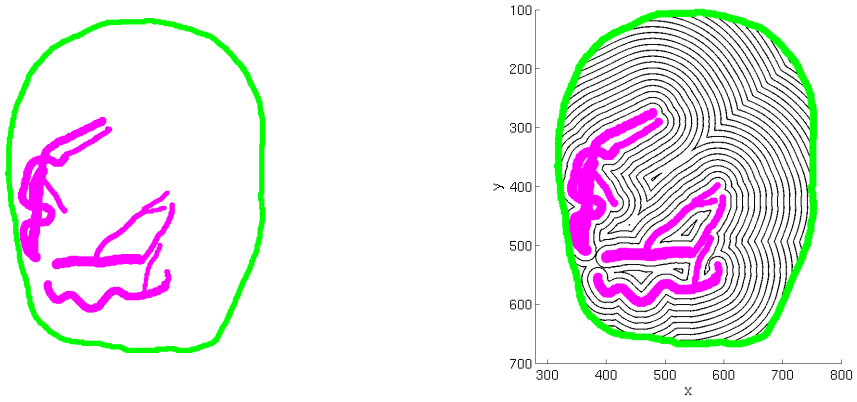

(a) Sample image with traced vessels.

(b) Contour plot of distance.

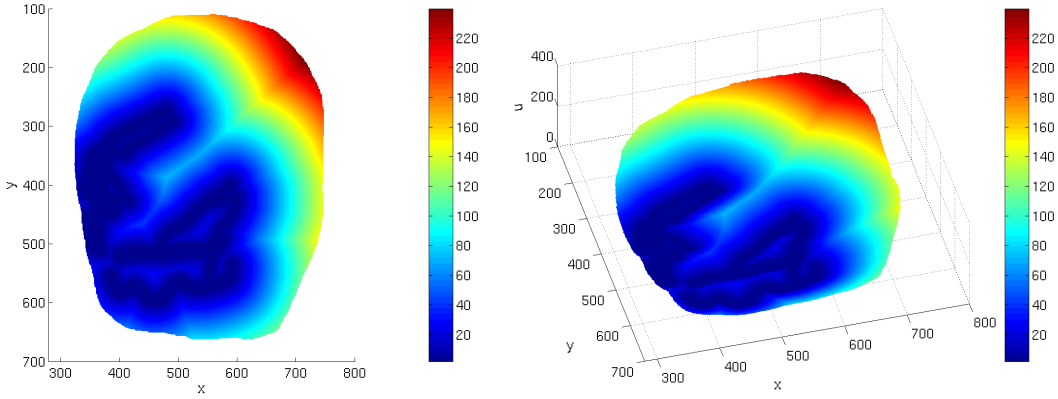

(c) Color plot of distance in 2D.

(d) Color plot of distance in 3D.

Figure 4.6: Plot of distance to the nearest vessel with poor coverage.

Measure 1 (M1) Mean distance divided by the maximum diameter D of the chorionic plate

$$M1 = \frac{\bar{u}}{\max(D)}.$$

Measure 2 (M2) Mean distance divided by the square root of the chorionic plate area A

$$M2 = \frac{\bar{u}}{\sqrt{A}}.$$

Measure 3 (M3) Mean distance divided by the chorionic plate area over the maximum

diameter of the chorionic plate

$$M3 = \frac{\bar{u}}{A/\max(D)}.$$

Relative Branching Coverage (RBC) We notice that these resulting geometric measures are difficult to compare directly; we are generally not interested in the actual value of the measure but rather the value relative to that of images of other placentas. Thus we divide the value of the measure for each image by the average of this measure over all sample images. The result is a non-dimensional number around 1. If it is 1, it means that the vessel coverage is average; if it is below 1, it means the coverage is better than average. Finally if it is larger than 1, the coverage is worse than average. For example, for mean distance we call this relative branching coverage

$$\text{RBC} = \frac{\bar{u}}{\text{mean}_{\text{samples}}(\bar{u})}.$$

Relative Area of the Vessel (RAV) Just because two images give the same measurement (based on average distance), does not mean they are equally well-covered. The image with less vessels is covering more area per vessel. Thus we penalize measures according to the total amount of vessels. We define the *relative area of the vessel* by finding the ratio of total vessel area V to the area of the chorionic plate.

$$\text{RAV} = \frac{V}{A}.$$

Relative Branching Efficiency (RBE) We define the *relative branching efficiency* as the "relative branching coverage" times the "relative area of the vessel".

$$\text{RBE} = \text{RBC} \times \text{RAV}.$$

Energy Budget (EB) We also define the *energy budget* as the "relative branching coverage" plus a constant multiple of the "relative area of the vessel"

$$\text{EB} = \text{RBC} + \frac{1}{5}\text{RAV}.$$

We note that all of the above measures are non-dimentional. In the next section, we explore the relation between these simple measures and birth weight.

4.5 Data Analysis

The available sample images have been grouped into three different categories: normal birth weight, high birth weight and low birth weight with roughly 40 cases in each category.

The variables we are interested in are the measure M that we described in section 4.4 and the birth weight BW of the fetus. Is there a relationship between these two variables? To answer this question, we need to perform a correlation study.

Due to patient confidentiality, we can not present the raw data here. Therefore, in this section, we will describe the method and result with mock fetal birth weight. The real data suggests there is a statistically significant correlation between our measures and the birth weight, as discussed in Section 4.5.3.

4.5.1 Correlation Study

The relationship between the measure $M1$ and the birth weight BW of the fetus can be measured by the correlation coefficient r, which indicates the strength of the relationship (see e.g., [DWC04]).

Given n pairs of observations (x_i, y_i), for $i = 1 \dots n$, where $x_i \in M1$ and $y_i \in BW$. Let $\bar{x}$ denote the mean of the measure $M1$, and $\bar{y}$ denote the mean of the birth weight of the fetus,

$$\bar{x} = \frac{x_1 + x_2 + \cdots + x_n}{n} = \frac{\sum_{i=1}^{n} x_i}{n},$$

$$\bar{y} = \frac{y_1 + y_2 + \cdots + y_n}{n} = \frac{\sum_{i=1}^{n} y_i}{n}.$$

Define

$$S_{xx} = \sum_{i=1}^{n} (x_i - \bar{x})^2 = \sum_{i=1}^{n} x_i^2 - \frac{(\sum_{i=1}^{n} x_i)^2}{n},$$

$$S_{yy} = \sum_{i=1}^{n} (y_i - \bar{y})^2 = \sum_{i=1}^{n} y_i^2 - \frac{(\sum_{i=1}^{n} y_i)^2}{n},$$

$$S_{xy} = \sum_{i=1}^{n} (x_i - \bar{x})(y_i - \bar{y}) = \sum_{i=1}^{n} x_i y_i - \frac{(\sum_{i=1}^{n} x_i)(\sum_{i=1}^{n} y_i)}{n}.$$

The correlation coefficient r is then computed by

$$r = \frac{S_{xy}}{\sqrt{S_{xx} S_{yy}}}.$$

The value $|r|$ indicates the strength of the linear association between the two variables. The most positive relationship is identified when $r = 1$, which means all (x_i, y_i) lie on a straight line with positive slope, and the most negative relationship is identified when $r = -1$, which means all (x_i, y_i) lie on a straight line with negative slope. There is less correlation between the variables when r is closer to zero.

4.5.2 Correlation Example

Given a sample of 43 placenta images, the measure $M1$ was computed. Mock birth weight (BW) was generated as

$$BW_i = aM1_i + b + X_i$$

where a, b specify a given linear relationship between Measure 1 ($M1$) and birth weight BW. Noise is added using X_i, an independent and identically-distributed random variable from a normal distribution with mean zero and standard deviation 0.05. Table 4.3 shows 43 samples with $a = -2.3$ and $b = 6.5$.

$M1$	BW	$M1$	BW	$M1$	BW	$M1$	BW
0.0222	6.4122	0.0275	6.4535	0.0165	6.4779	0.0283	6.5548
0.0261	6.4164	0.0249	6.4698	0.0172	6.4860	0.0180	6.4706
0.0309	6.4042	0.0254	6.4126	0.0212	6.4089	0.0221	6.4530
0.0208	6.4236	0.0176	6.4914	0.0148	6.5096	0.0242	6.3932
0.0380	6.3232	0.0313	6.3788	0.0253	6.4523	0.0217	6.4611
0.0464	6.3250	0.0211	6.4788	0.0214	6.5453	0.0290	6.4136
0.0331	6.3919	0.0296	6.3754	0.0202	6.3878	0.0145	6.4821
0.0289	6.5005	0.0219	6.5015	0.0273	6.3890	0.0172	6.4807
0.0248	6.4591	0.0130	6.4112	0.0229	6.3939	0.0212	6.5241
0.0284	6.4368	0.0292	6.3773	0.0235	6.4489	0.0408	6.3948
0.0299	6.5055	0.0203	6.4303	0.0211	6.5008		

Table 4.3: M1 values and mock BW data.

Figure 4.7 shows a scatter plot of the mock data. The straight line indicates the linear best fit. The r value -0.54882 shows a statistically significant correlation between the Measure 1 and mock birth weight.

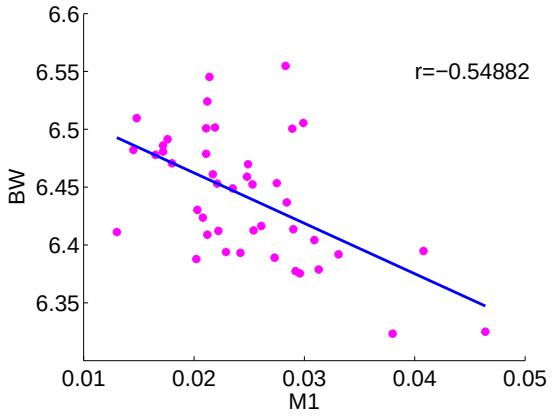

Figure 4.7: Scatter plot of M1 and mock BW.

4.5.3 Correlation of Real Data

The birth weight data is not presented here for reasons of patient confidentiality. However, Table 4.4 shows a preliminary correlation study between our measures and fetal birth weight. We note statistically significant correlation between RBC and BW and between EB and BW. On the other hand RBE is not correlated with BW. This is a preliminary result based on a sample of 43 placentas corresponding to normal birth weights. Research and analysis on abnormally low and high birth weights is ongoing.

	relative branching coverage	relative branching efficiency	energy budget
birth weight	-.424	.019	-.378

Table 4.4: Correlation Study on real data.

Chapter 5

Image Segmentation

We can perform the calculations described in Chapter 3 when we have a simple ideal image like Figure 2.1. From a true digital image of a placenta (e.g., Figure 1.2), it is not easy to obtain information such as vessel location Γ, which we need to apply the boundary conditions. Currently, we rely on a trained technician to analyze and segment the images by hand.

We investigate capturing the blood vessels automatically by applying de-noising and segmentation techniques on the chorionic plate. Basic tools for image processing include de-blurring, de-noising, segmentation and others [AK06].

5.1 Manual Segmentation

A pathologist or a trained technician uses digital image manipulation software [GT] to trace the blood vessels, umbilical cord attachment point, boundary of the placenta, the penny, and some marker points on the ruler. Each of these features is marked with a different unique color which can then be located by our code. This manual segmentation is expensive, and the geometric information which have been obtained may not be objective in the sense of not being reproducible by another individual. That is, for a large sample size of many images, the same technician would likely have to trace all of the images to avoid bias.

5.2 De-blurring

De-blurring is a process to enhance a blurry image by sharpening it. One idea is to use an unsharp mask, which essentially subtracts the blurred image from the original one [GW02]. Figure 5.1 shows an example of de-blurring using an unsharp mask. In Figure 5.2, de-blurring is applied to a placenta image and the image did not get clearer, but instead some noise was introduced. This is probably because the image was not blurry to begin with.

Figure 5.1: Left: example blurry image. Right: de-blurred image by performing an unsharp mask. Example image by Pincel3D, Creative Commons licensed.

5.3 De-noising

Noise is typically random values from some distribution added to some of the pixels in an image. In Figure 5.3, noise has been deliberately added to the image and then de-noising applied using one possible technique called a median filter [GW02], which replaces the value of a pixel by the median of the gray levels in the neighborhood of that pixel.

However from Figure 5.4 we can see that our original image is already clear enough,

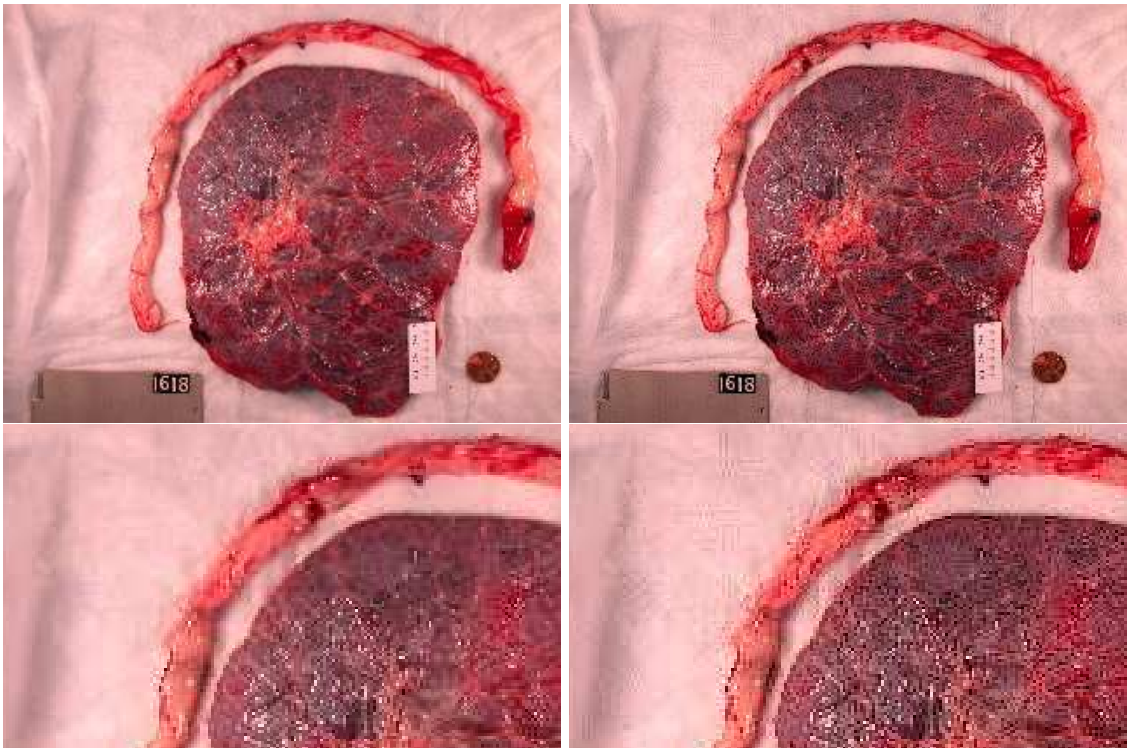

Figure 5.2: Top row: original image (left), de-blurred image by performing an unsharp mask (right). Bottom row: zoomed in versions of above.

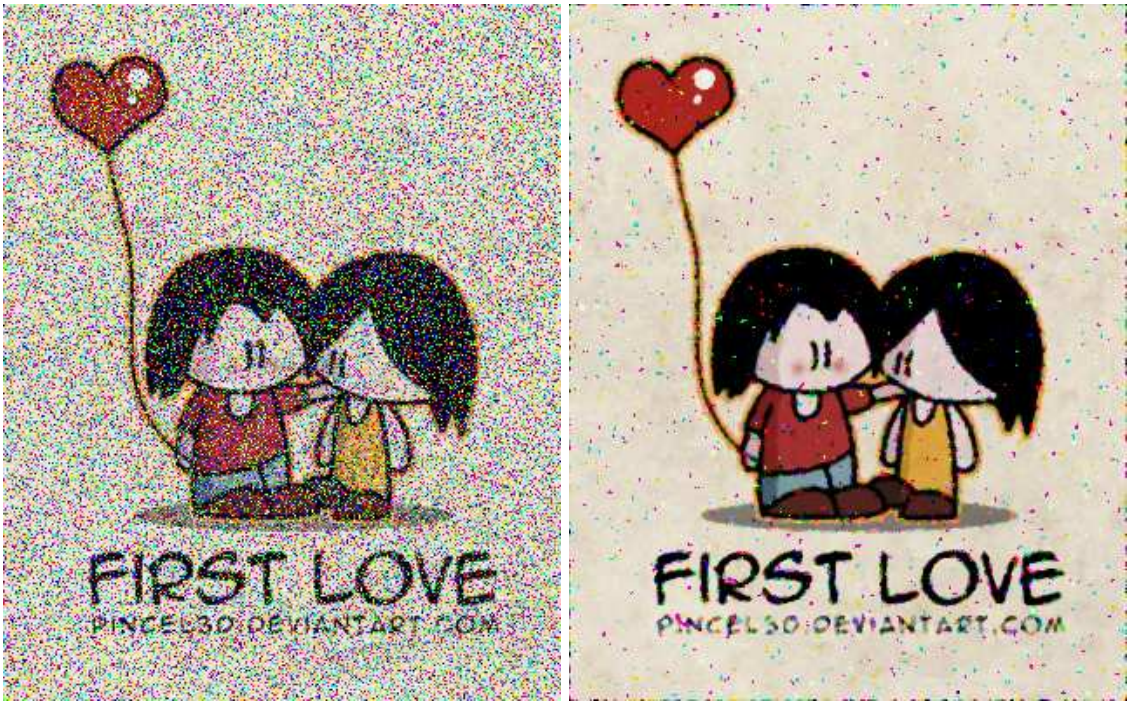

Figure 5.3: Left: sample noisy images ("salt and pepper" noise [GW02] artificially added to each RGB channel). Right: de-noised image by performing median filter. Example image by Pincel3D, Creative Commons licensed.

after we apply de-noising, it did not change much except some small reflection effects from the camera flash were removed and the image was blurred slightly.

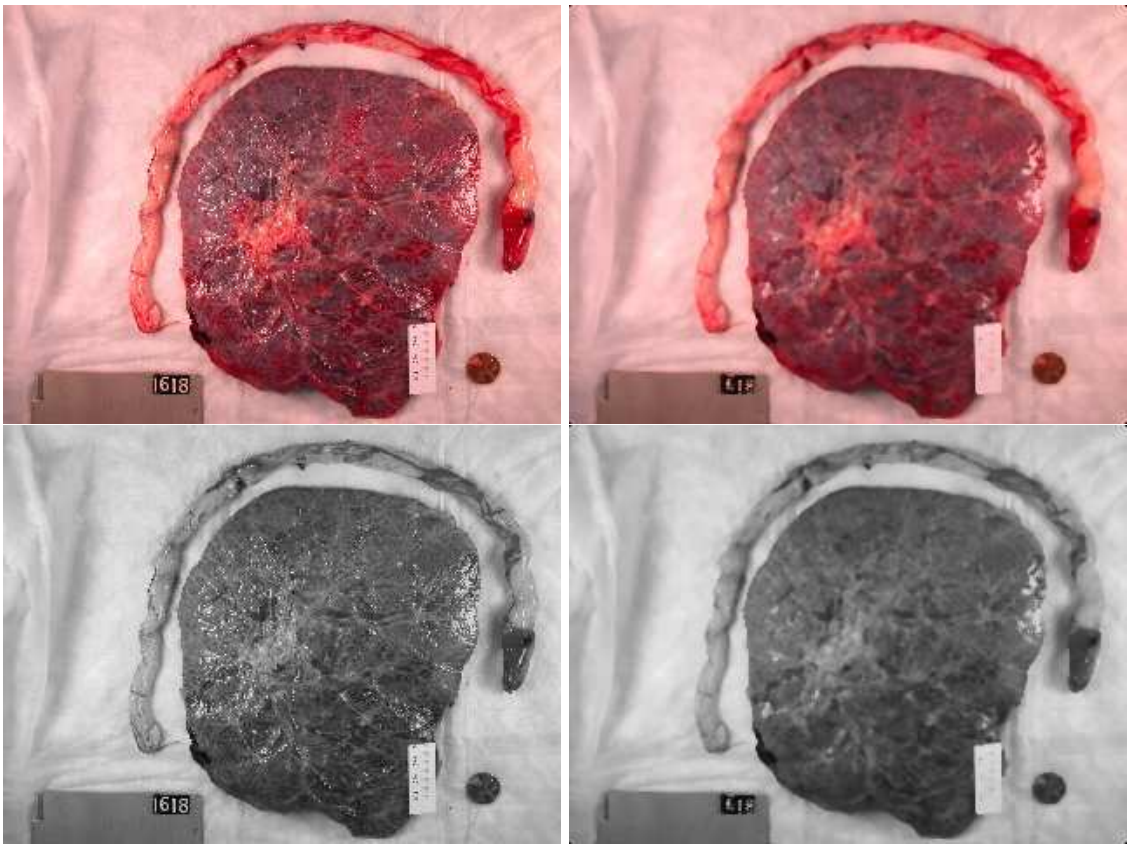

Figure 5.4: Top row: original image (left), de-noised image by performing median filter (right). Bottom row: grey scaled versions of above.

5.4 Segmentation

The idea of segmentation is to find ("mark") different objects in an image. In our image, we can easily visually spot a placenta, a penny, a ruler etc, and it should be relatively straightforward to automatically segment these objects. However a more challenging problem would be to segment out the vessels because visually it is less clear which parts of the image are the vessels and which are the chorionic disc. Indeed, this task may requires expert knowledge from a trained pathologist. Currently, the manual segmentation is done by human operator, ideally it could be combined with automatic approaches to make an interactive

segmentation. The following sections outline several techniques that might be useful.

5.4.1 Active Contours (Snakes) Method

The active contour (snakes) method [KWT88] uses gradient information to find the edges of the objects. Based on intensity, we partition the image by calculating the gradient for every pixel on the image. The gradient is a vector at each pixel which points in the direction of the greatest intensity change. The magnitude of the gradient reflects how fast the intensity changes near each pixel. Figure 5.5 shows the gradient magnitude can clearly indicate the edge of the penny and placenta, but does not seem to give enough information about the vascular structure. Thus, we expect this method will not work well.

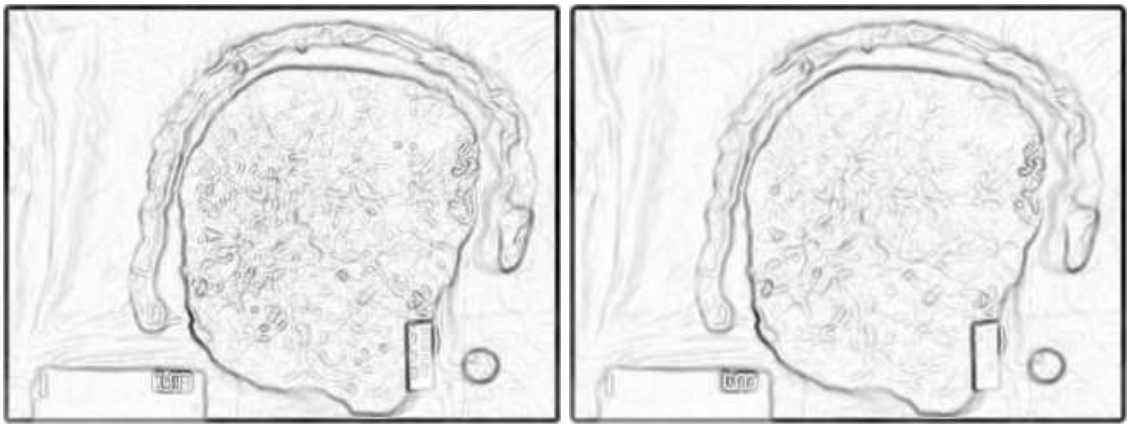

Figure 5.5: Left: edge detected from the original grey scaled image. Right: edge detected from de-noised grey scaled image.

5.4.2 Active Contours without Edges

An alternative approach to segmentation is "active contour without edges" [CV01] which does not directly rely on gradient information. However the algorithm as given in [CV01] is intended to segment out objects which have both insides and outsides. The vessel structure is made of curves, thus it does not have this property. We do not expect this method to work well for the placenta images. Indeed, Figure 5.6 shows the segmentation has done a reasonable job of identifying the chorionic plate, the umbilical cord and the penny. However, no useful information about the blood vessels can be seen.

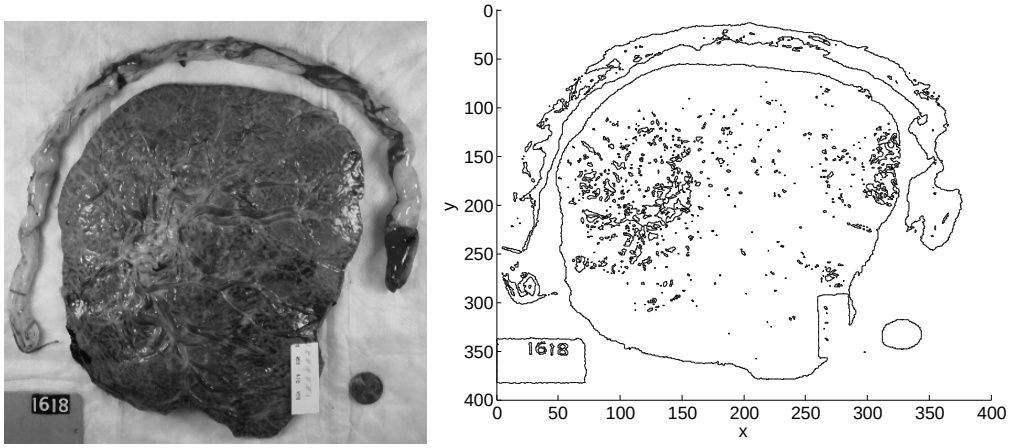

Figure 5.6: Left: grey scaled image. Right: active contours without edges applied to the left image. Computation performed using the code of Luke Tian [Tia].

One possibility for future study is to look for algorithms for segmenting tree-like structures consisting of curves.

5.5 Shape-from-shading

The idea of shape-from-shading is to recover three-dimensional information about shape from a two dimensional black-and-white image. This is not a well-posed problem but [RT92] introduced the "viscosity solution" approach which is very interesting. We implemented the algorithm following [RT92] and some results are shown in Figure 5.7.

From Figure 5.7, we can see the position of the penny (small cone in the front right corner of (a)) and the placenta appears as a "mountain", but we can not see any useful information about the vessels. Thus, shape-from-shading does not seem to be suitable for getting vessel information from our current placenta images. It works better on images containing objects of the same material, where the shade on the image is only effected by the lighting sources from the camera flash [RT92]. However, that is not the case here, the placenta images we study are made up of different materials with different colours.

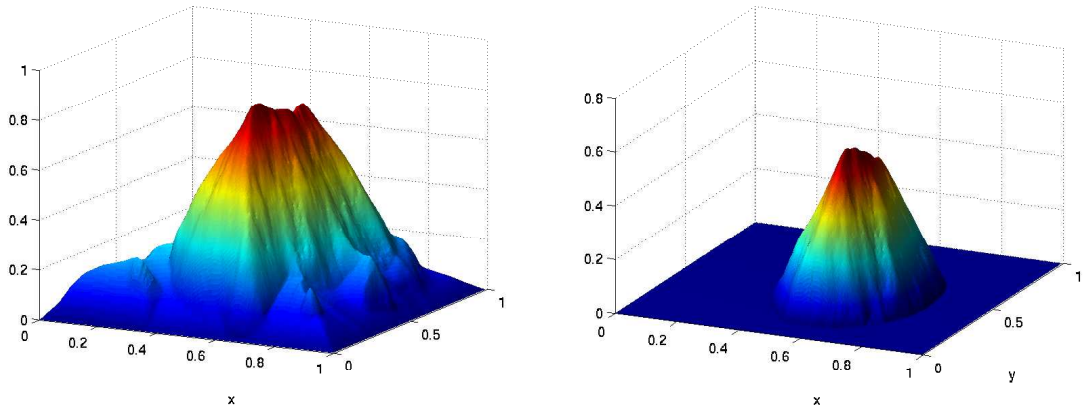

(a) (b)

Figure 5.7: Left: shape from shading applied to the original image. Right: shape from shading only applied to the placenta.

Chapter 6

Conclusions

A model was implemented for measuring the branching properties of the blood vessels of the placenta on the chorionic plate. The model is based on computing the distance from any point of the placenta to the nearest blood vessel. Using this model, we showed preliminary evidence of correlation between chorionic plate blood vessel geometry and the birth weight of infants.

The images were first traced manually by a pathologist. This provided an outline of the chorionic disc and the location of the major blood vessels. The process also identified a penny and markings on a ruler for use in scaling the images. Computing the distance u from every point in the chorionic plate was performed by numerically solving the eikonal equation $|\nabla u| = 1$ on a 2D domain consisting of the irregularly shaped chorionic plate. Boundary conditions imposed $u = 0$ on the blood vessels themselves. Several numerical approaches for solving the eikonal equation were evaluated including time-dependent and iterative methods. The fast sweeping technique [TCOZ03] turned out to be particularly efficient and straightforward to implement. The computed distance was then averaged in various ways to obtain measurements of the blood vessel coverage. These measurements were made non-dimensional by scaling based on the diameter of a penny appearing in most images.

Several approaches for the automatic tracing (segmentation) of the blood vessels on placental images were investigated. The placental images had no obvious errors from noise and thus denoising was deemed unnecessary. Edge detection techniques based on the gradient of the image were unreliable due to lack of contrast between the blood vessels and surrounding tissue. Shape from shading [RT92] was also not effective, likely because of the presence of

both texture and colour information in the images. Currently we rely on human to trace or pick out the vessels, and we would like this to be automated or semi-automated. Thus the automatic segmentation problem warrants further investigation.

To summarize, in consultation with a pathologist, we successfully developed and implemented simple metrics for vasculature coverage of the chorionic plate. Specific medical results using our measures will appear in [Sal08] and [HLOS].

Bibliography

[ABD+08] Morten Andersen, David Belanger, Radina Droumeva, Jenny Li, Gilbert Moss, and Gabriela Palau. Quantifying clinically significant features of placental histology images: a method. Technical report, MITACS Summer School in Industrial Mathematics, August 2008.

[ACI98] Balu H. Athreya, May L. Cheh, and Lawrence C. Kingsland III. Computer-assisted diagnosis of pediatric rheumatic diseases. *Pediatrics*, 102(4):e48, October 1998.

[AK06] Gilles Aubert and Pierre Kornprobst. *Mathematical Problems in Image Processing: Partial Differential Equations and the Calculus of Variations*, volume 147 of *Applied Mathematical Sciences*. Springer-Verlag, second edition, 2006.

[Bar97] David J.P. Barker. Maternal nutrition, fetal nutrition, and disease in later life. *Nutrition*, 13(9):807–813, September 1997.

[BF00] Richard L. Burden and J. Douglas Faires. *Numerical Analysis*. Brooks Cole, seventh edition, 2000.

[CV01] Tony F. Chan and Luminita A. Vese. Active contours without edges. *IEEE Transactions on Image Processing*, 10(2):266 – 277, Feburary 2001.

[DWC04] Shirley Dowdy, Stanley Wearden, and Daniel Chilko. *Statistics for research*. Wiley, third edition, 2004.

[Eva98] Lawrence C. Evans. *Partial Differential Equations*, volume 19 of *Graduate Studies in Mathematics*. American Mathematical Society, 1998.

[GK06] P.A. Gremaud and C.M. Kuster. Computational study of fast methods for the eikonal equation. *SIAM Journal on Scientific Computing*, 27(6):1803, 2006.

[GNS+08] Steven G. Gabbe, Jennifer R. Niebyl, Joe Leigh Simpson, Henry Galan, Laura Goetzl, Eric R.M. Jauniaux, and Mark Landon. *Obstetrics: Normal and Problem Pregnancies*. Elsevier, fifth edition, 2008.

[GT] The GIMP Team. GIMP - the GNU Image Manipulation Program.

[GW02] Rafael C. Gonzalez and Richard E. Woods. *Digital Image Processing*. Prentice Hall, 2002.

[HLOS] Danielle Haas, Jenny Li, Adam Oberman, and Carolyn Salafia. Computational placental pathology: Using placental geometry to assess placental function. In preparation.

[HNF08] Health on the Net Foundation. `http://debussy.hon.ch/cgi-bin/HONselect?browse+E01.158`, 2008. Accessed 2008-10-07.

[HT05] Shu-Ren Hysing and Stefan Turek. The eikonal equation: numerical efficiency vs. algorithmic complexity on quadrilateral grids. In *Algoritmy*, pages 22–31, 2005.

[KWT88] Michael Kass, Andrew Witkin, and Demetri Terzopoulos. Snakes: Active contour models. *International Journal of Computer Vision*, 1(4):321–331, January 1988.

[RP07] Sabine Raab and Karl H. Plate. Different networks, common growth factors: shared growth factors and receptors of the vascular and the nervous system. *Acta Neuropathologica*, pages 607–626, May 2007.

[RT92] Elisabeth Rouy and Agnès Tourin. A viscosity solutions approach to shape-from-shading. *SIAM Journal on Numerical Analysis*, 29(3):867–884, June 1992.

[Sal08] Carolyn Salafia. Chorionic vascular branching affects placental efficiency and birth weight independent of placental weight, 2008. 16th World Congress for the study of hypertension in pregnancy.

[Set99] James A. Sethian. *Level Set Methods and Fast Marching Methods: Evolving Interfaces in Computational Geometry, Fluid Mechanics, Computer Vision, and Materials Science*. Cambridge University Press, 1999.

[SMT+05] Carolyn M. Salafia, Elizabeth Maas, John M. Thorp, Barbara Eucker, John C. Pezzullo, and David A. Savitz. Measures of placental growth in relation to birth weight and gestational age. *American Journal of Epidemiology*, 162(10):991–998, 2005.

[SV90] Carolyn M. Salafia and Anthony M. Vintzileos. Why all placentas should be examined by a pathologist in 1990. *American Journal of Obstetrics and Gynecology*, 163(4):1282–93, October 1990.

[TCOZ03] Richard Tsai, Li-Tien Cheng, Stanley Osher, and Hong-Kai Zhao. Fast sweeping algorithms for a class of Hamilton-Jacobi equations. *SIAM Journal on Numerical Analysis*, 41(2):673–694, 2003.

[Tia] Luke Tian. Master's thesis, Simon Fraser University. In preparation.

[YSS+08] Michael Yampolsky, Carolyn M. Salafia, Oleksandr Shlakher, Danielle Haas, Barbara Eucker, and John Thorp. Modeling the variability of shapes of a human placenta. *Placenta*, 29(9):790–797, September 2008.

[Zha05] Hongkai Zhao. A fast sweeping method for eikonal equations. *Mathematics of Computation*, 74:603–627, 2005.